JOURNAL OF GEOPHYSICAL RESEARCH, VOL. 101, NO. E10, PAGES 23,063–23,076, OCTOBER 25, 1996

Mapping Precambrian structures in the Sahara Desert with SIR-C/X-SAR radar: The Neoproterozoic Keraf Suture, NE Sudan

Mohamed G. Abdelsalam and Robert J. Stern

Center for Lithospheric Studies, University of Texas at Dallas, Richardson

Abstract. A major N-trending Neoproterozoic suture between composite arc terranes of the Arabian-Nubian Shield in the east and older crust of the Nile Craton to the west is inferred to trend N-S close to the Nile in northern Sudan. We used shuttle imaging radar (SIR) C/X synthetic aperture radar (SAR) imagery to find and map these structures in the poorly known Keraf Suture which are not apparent on visible or near IR imagery due to extensive sand cover. *L* band (23 cm wavelength) radar images best resolve geologic structure; the other frequencies of the SIR-C/X-SAR system (*X* and *C* bands) permit qualitative evaluation of the effects of surface versus subsurface backscattering. Interpretation of *L* band images supported by field work indicates that the Keraf Suture is ~50 km wide and >550 km long, making it the longest basement structure recognized to date in NE Africa. The northern part of the Suture comprises ophiolitic rocks which were thrust westward over tightly folded sediments of the Nile Craton. The southern Keraf Suture is dominated by N- and NNW-trending, left-lateral strike-slip faults that affect previously deformed passive margin sediments. Associated with these faults are NE-trending transpressional folds and a possible transtensional basin. These structures are interpreted to be due to NW-SE oblique collision between the Arabian-Nubian Shield and the Nile Craton, as east and west Gondwana collided in the last 150 m.y. of Neoproterozoic time.

Introduction

The supercontinent of Greater Gondwana formed by collision between east and west Gondwana during late Neoproterozoic time, about 650 Ma [*Stern*, 1994]. Collision between east and west Gondwana resulted in the formation of the ~5000 km long East African Orogen (Figure 1) which comprises the Arabian-Nubian Shield (ANS) in the north and the Mozambique Belt to the south [*Stern*, 1994]. Collision took place between ~700 and 650 Ma and may have had continued up to ~550 Ma after the consumption of the Neoproterozoic "Mozambique Ocean" (Figure 1). The most intense continental collision occurred to the south in the vicinity of present Madagascar, Tanzania and southern Kenya, where crustal thickening led to the formation and exhumation of extensive tracts of high-grade metamorphic rocks [*Key et al.*, 1989; *Muhongo and Lenoir*, 1994]. Collision was less intense in the north, resulting in less crustal thickening and denudation. In this region, remnants of the ancient Mozambique Ocean are preserved as intra-oceanic island arc/back-arc/ophiolite assemblages of predominantly greenschist-facies metamorphic grade which now define the ANS [*Burke and Sengor*, 1986].

Neoproterozoic crust in the ANS consists of ~900-550 Ma old assemblages of dismembered arc volcanics, immature sediments, and ophiolites similar to modern arc and back-arc basin complexes. Geochronologic and isotopic data indicate that the parts of the ANS now preserved in the Red Sea Hills of Sudan (Figure 2) were accreted during Neoproterozoic time [*Stern and Kröner*, 1993]. These sequences make up terranes that were welded together along E- to NE-trending arc-arc ophiolite-decorated sutures (Figure 2) [*Stern*, 1994]. Juvenile crust of the ANS super-terrane was intruded by granodioritic batholiths and sandwiched between older continental fragments of east and west Gondwana (Figure 1).

We are particularly interested in the western boundary of the ANS with West Gondwana because this zone preserves structures and rock sequences that are fundamental for understanding the evolution of the East African Orogen. West Gondwana in NE Africa comprises older crust of the Nile Craton, which, although pervasively deformed and intruded by plutons during the Neoproterozoic, appears to be the northern extension of the Congo Craton [*Sultan et al.*, 1994]. Geochronological and isotopic data suggest that gneiss of the Nile Craton is predominantly Paleoproterozoic or Mesoproterozoic in age [*Harris et al.*, 1984; *Schandelmeier et al.*, 1988; *Harms et al.*, 1990; *Stern et al.*, 1994]. Neoproterozoic deformation of the Nile Craton includes greenschist- to amphibolite-facies metamorphism and emplacement of granitic plutons [*Ries et al.*, 1985; *Stern et al.*, 1994] as well as opening and closing of aulacogen-like oceanic re-entrants such as the Atmur-Delgo Suture (Figure 2) [*Abdel-Rahman* et al., 1990; *Schandelmeier et al.*, 1994; *Denkler et al.*, 1994; *Harms et al.*, 1994; *Stern et al.*, 1994) .

Previous workers have defined the location of the boundary between the ANS and the Nile Craton on the basis of lithologic or isotopic differences [*Vail*, 1983, 1985; *Almond and Ahmed*, 1987; *Stoeser and Stacey*, 1988; *Schandelmeier et al.*, 1988; *Dixon and Golombek*, 1988; *Sultan et al.*, 1990; 1992; 1994; *Abdelsalam and Dawoud*, 1991]. The location, nature, and tectonic evolution of the suture separating the ANS and the

Paper number 96JE01391.
0148-0227/96/96JE-01391$9.00

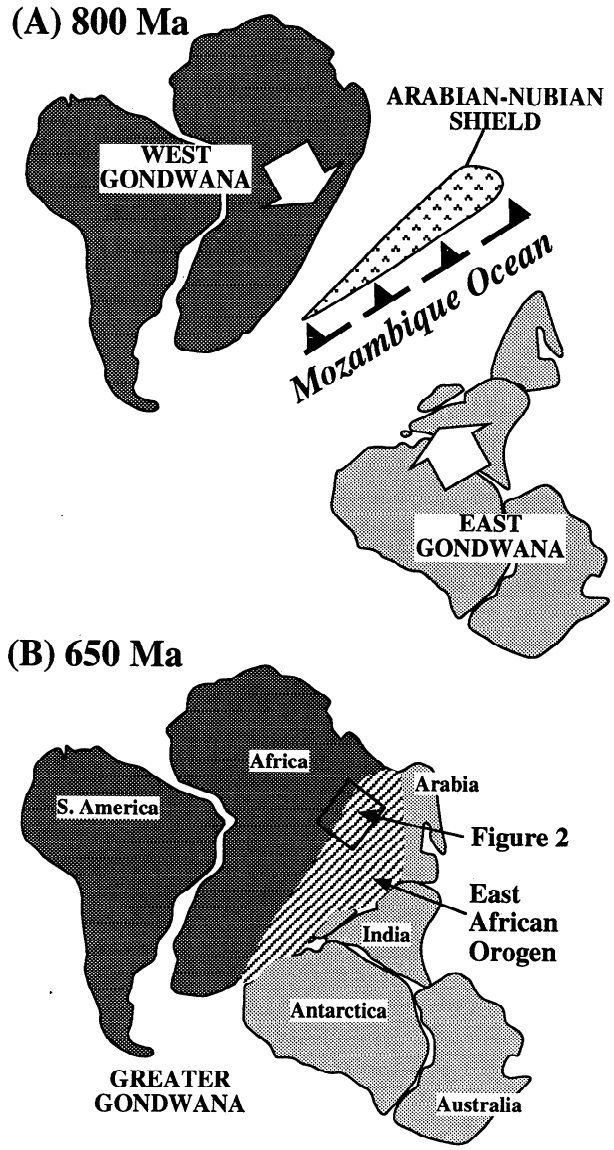

Figure 1. Simplified reconstruction of the formation of Greater Gondwana during the Neoproterozoic. (a) The Mozambique Ocean and the composite terrane of the ANS lie between East and West Gondwana. (b) East and West Gondwana collide to form Greater Gondwana with the East African Orogen marking the collision zone.

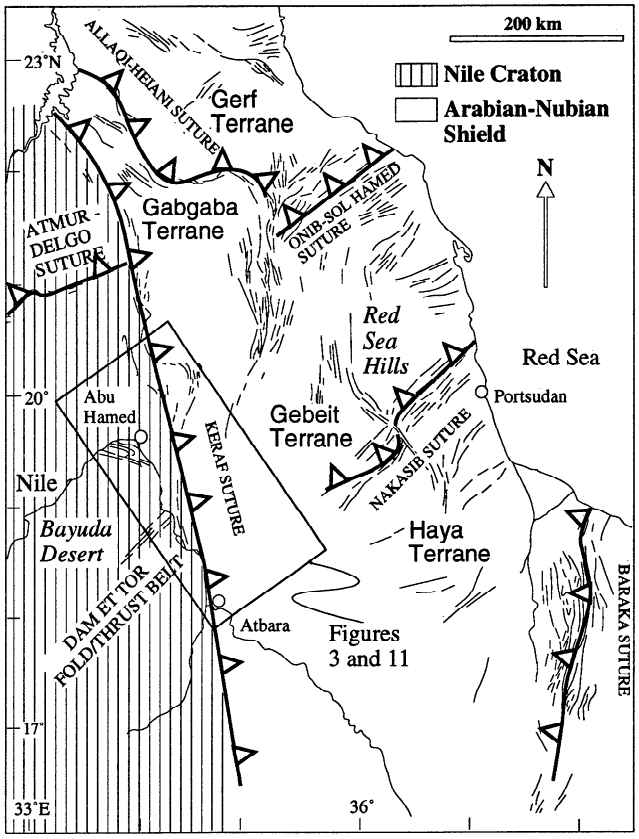

Figure 2. Tectonic setting of the Keraf Suture between the Nile Craton and the Arabian-Nubian Shield.

Nile Craton itself remain poorly understood, however, because it has never been directly studied. The above-mentioned data sets indicate that the boundary between the Nile Craton and the ANS extends N-S along longitude 33-34°N, so recent efforts have focused on the appropriate meridional structure. This structure was called the Keraf Zone by *Almond and Ahmed* [1987]. The Keraf Zone north of Abu Hamed (Figure 2) is ~50 km wide and is defined by sub-vertical foliation and tight folds which deform supracrustal rocks dominated by carbonate-rich turbidites [*Stern et al.,* 1993]. Mapping of ophiolitic rocks in the eastern Keraf Zone indicates that it is probably a suture, which *Abdel-Rahman* [1993] named the Keraf Suture and interpreted it as a result of closing of an oceanic basin to the east. *Abdelsalam et al.* [1995] used SIR A radar images along with field investigations to reconstruct the structural evolution of the northern Keraf Suture and suggested that it is the fundamental suture between the ANS and the Nile Craton. They also suggested that the suture developed during NW-SE oblique collision between east and west Gondwana. Oblique shortening caused by this collision was partitioned into N-trending upright folds, and subordinate NW-trending, left-lateral and NE-trending, right-lateral strike-slip faults.

The continuation of the Keraf Suture to the south has remained unknown due to burial of basement structures beneath the extensive aeolian sand cover of the Sahara Desert. The vicinity of the study area between the Nile River and the Red Sea Hills (Figure 2) is characterized by low relief except for a few isolated inselbergs. Strong north winds deposit and rework a thin blanket of sand and silt over the subdued basement outcrops. We report here a first look at the basement structures of the southern Keraf Suture, made possible by shuttle imaging radar (SIR) C/X synthetic aperture (SAR) imaging of the region. We used the radar images to (1) produce a regional map of the structural features of the southern Keraf Suture, (2) guide field work to check these interpretations and collect structural data, and (3) produce geological and structural maps for key areas which are critical for understanding the tectonic evolution of this part of the Keraf Suture. These maps were produced by interpreting the SIR C/X SAR images along with ground data. This report is intended to (1) document the utility of multifrequency, multipolarization radar imagery for mapping poorly exposed and shallowly buried basement structures in hyper-arid regions, (2) trace the southern continuation of the Keraf Suture and decipher its structural

evolution, and (3) define the role of the Keraf Suture during the collision between East and West Gondwana near the end of Precambrian time.

Physiography of the Southern Keraf Suture

The three geologic provinces studied here namely, the Nile Craton, southern Keraf Suture, and ANS, have distinct physiographic expressions (Figure 3). These differences partly reflect varied resistance to erosion, accentuated by the location of the Nile River along the Keraf Suture. The Nile Craton in the vicinity of the study area underlies the Bayuda Desert, an area of well-exposed basement that extends west of the Nile River. Amphibolite-facies gneiss and supracrustal rocks dominate exposures in the Bayuda Desert. Better exposure of basement rocks here is due largely to trapping of south-migrating aeolian sand sheets by the Nile River as it extends WSW from Abu Hamed (Figure 2). The good exposures in the Bayuda

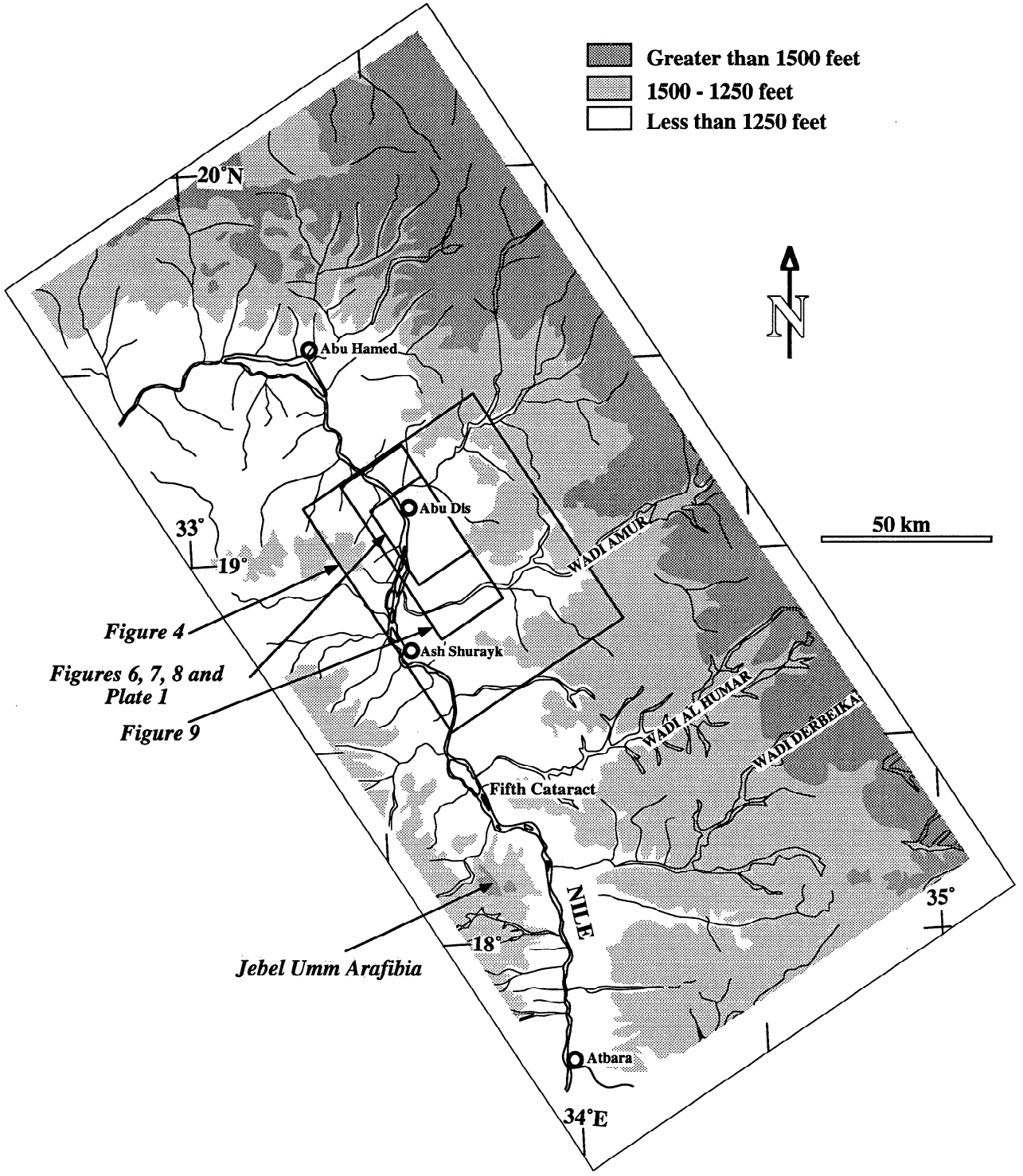

Figure 3. Physiographic summary map of the study area based on topographic maps published in 1985 by the Defence Mapping Agency Aerospace Center (St. Louis, Missouri). The outline of areas covered by Figures 4, 6, 7, 8, 9, and plate 1 are shown by solid rectangles. The map covers the same area covered by Figure 10.

Desert are also due to the moderate relief of the region, with a maximum of 150 m. Sand cover is more extensive in areas with less than 150 m relief (Figure 3). The Bayuda Desert has also been the site of late Cenozoic uplift, which is expressed by scattered alkalic volcanic centers that range in age from mid-Miocene to Pleistocene [*Barth et al.*, 1983], including the extinct Jebel Umm Arafibia near the southern end of the study area (Figure 2). This uplift has probably been responsible for the deflection of the Nile River around the Bayuda Desert.

The ANS is exposed in the Red Sea Hills east of the Keraf Suture. This is an area of rugged relief, with closely-spaced mountain ranges that rise several hundred meters above the floors of the surrounding drainages. Exposures are excellent and visisble and near ifrared (VNIR) imagery such as Landsat Thematic Mapper (Landsat TM) has proven to be extremely useful in reconstructing the tectonic history of this region [e.g. *Sultan et al.*, 1993]. The western margin of the Red Sea Hills physiographic province is poorly defined, but this lies well to the east of the Keraf Suture.

The southern Keraf Suture lies between the Red Sea Hills and the Bayuda Desert in a 100 km wide peneplain described by *Raisz* [1952] as "Rock, sand, and gravel flats with few inselbergs and traces of dendritic river courses". *Sandford* [1949] identified this peneplain as the lower of two erosional surfaces developed in northern Sudan lying 400±50 m above sea level, and suggested that this surface was lower Tertiary to Recent in age. Our field studies in the region indicate that it is characterized by a subdued relief that is largely covered by sand and small dunes (Figure 4). Basement outcrops are scarce and typically act to trap windblown sand. Basement lithologies are dominated by amphibolite-facies supracrustal rocks which include paragneiss (~55% of outcrops), metacarbonates (~40%), and amphibolite and mafic-ultramafic rocks (~5%).

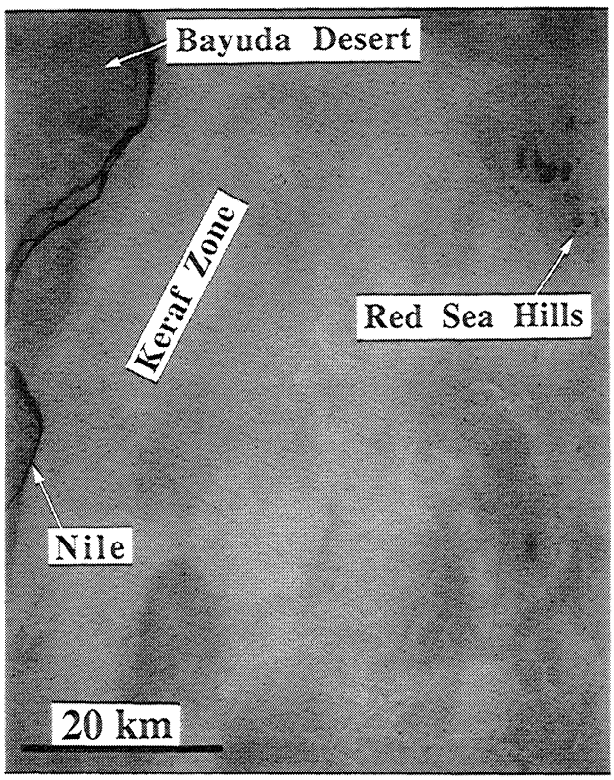

Figure 4. Shuttle hand-held photograph showing the Keraf Suture from space. See location in Figure 3.

We interpret these as being part of the same passive margin sequence found in the northern Keraf Suture (*Stern et al.*, 1993).

Four physiographic types are recognized within the study area of the southern Keraf Suture which include (1) inselbergs (Figure 5a), (2) undulating basement plain (Figure 5b), (3) low-lying outcrops, partially covered by sand (Figure 5c), and (4) plains covered by sand sheets (Figure 5d). These physiographic types are associated with distinct lithologies, based on our field studies and have characteristic tones and textures in the SIR C/X SAR images. Therefore SIR C/X SAR images can be used to map lithology as well as structure, which is discussed below.

SIR-C/X-SAR Images

The SIR C/X SAR images used in this study were developed at the Jet Propulsion Laboratory (JPL), in Pasadena, California. Black and white, single-band images; black and white, ratio-band images; and color-composite, multiband images were developed using standard procedures established at JPL to read-in digital data from tapes, convert data into byte images, enhance images, co-register the SIR C and the X SAR data, and produce color-composite, multiband images. Information for individual images are given in figure captions. The SIR C/X SAR images in general proved to be far superior in revealing structural detail in the Keraf Suture over the wide range of visible and near-infrared imagery that we examined (Landsat TM, Shuttle hand-held photography, and aerial photographs) (Figure 6). The wavelength and polarization of the radar bands used in the SIR C/X SAR images are limiting factors for resolving structural features. In the following discussion, we examine the strengths and weaknesses of the various radar wavelengths and polarizations for resolving structures within a 18 km x 23 km test region in the Keraf Suture.

Black and white, *L* band (wavelength 24 cm), *C* band (wavelength 6 cm), and *X* band (wavelength 3 cm), and black and white *L/C* ratio images are used to test the usefulness of SIR C/X SAR data for revealing geological structures. Polarizations vertically transmitted and vertically received(vv), horizontally transmitted and horizontally received (hh), and horizontally transmitted and vertically received(hv) are used for *L* and *C* bands. These are abbreviated as L_{vv}, L_{hh}, L_{hv}, C_{vv}, C_{hh}, and C_{hv} band or image. X SAR had only one polarization (vv). These images are referred to as *X* band or image. Black and white, ratio-band *L/C* images with *L* and *C* bands of different polarizations are used. These are referred to as L_{vv}/C_{vv} and L_{hh}/C_{hh} ratio or image.

L_{vv}, L_{hh}, and L_{hv} images are of similar quality and better reveal structures than *C* or *X* images (Figure 7). Radar penetrates dry sand for a constant number of wavelengths, and estimates of *L* band penetration of dry, well-sorted sand are on the order of 1 to 6 m [*McCauley et al.*, 1982]. Thus the better resolution of structure is attributed to deeper penetration of sandy cover by the *L* band such that it is more completely reflected from underlying basement. Our field investigations indicated that the *L* image (Figure 7a) shows structural details of basement buried under less than 2 m of sand. Regions where the basement is buried beneath more than 2 m of sand cover show up as dark areas in *L* images (Figure 7a). These areas are mostly small wadis; it is possible that radar penetration is also decreased by subsurface moisture in these channels.

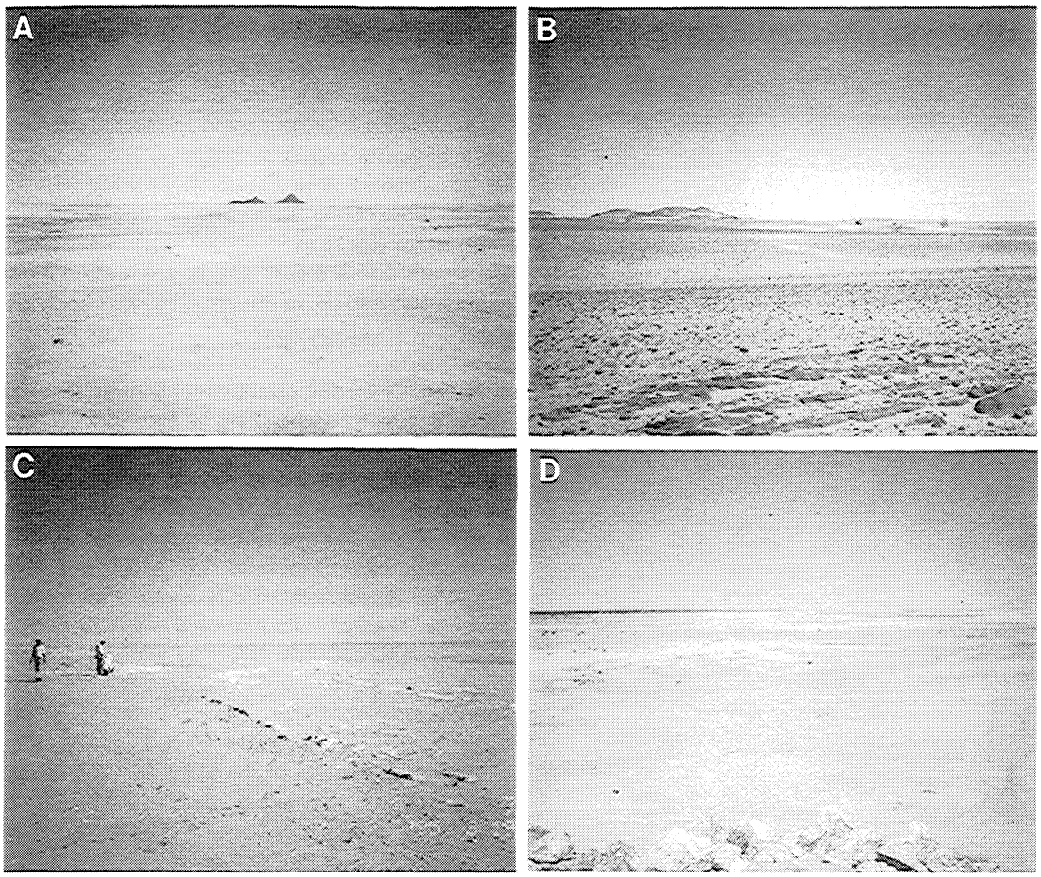

Figure 5. Ground photographs showing physiographic types in the Keraf Suture: (a) inselbergs, (b) undulating basement plain, (c) low-lying outcrops, partially covered by sand, and (d) plains covered by sand sheets.

C and *X* images are of limited use in mapping structural details in areas where basement is partially covered by sand (Figure 7) owing to their limited penetration capability. However, the *C* and *X* images are useful for outlining physiographic features such as drainages (Figure 7b and 7c). An interesting effect is seen when like-polarization (vv and hh) and cross-polarization (hv) *C* images are compared (Figure 8). The C_{hv} image (Figure 8b) reveals basement structural features better than C_{vv} (Figure 7b) and C_{hh} (Figure 8a) images. Correspondingly, the like-polarization *C* images better reveal details of the drainage system. These observations suggest that cross-polarization enhances the capability of the radar to penetrate hyper-arid sand. The fact that this effect is not seen in the *L* images may be because both like-polarization and cross-polarization *L* images effectively penetrate the cover to reveal the basement.

The L_{vv}/C_{vv} image is diffuse and does not resolve structures well (Figure 7d). It does, however qualitatively map relative penetration by *L* band versus *C* band. Three parts of the area are dark (Figure 7d), corresponding to a low *L/C* ratio. The Nile River is dark because it is a specular reflector for both *L* and *C* bands. Areas of good outcrop (such as the N-trending ridge visible in the upper center of Figures 6a and 6b, and 7a-7c) are dark because backscattering of both wavelengths by the surface is similar. Similarly, flat areas with thick sediment fill (which prevents both *L* and *C* bands from penetrating and backscattering from basement relief underneath) appear dark in *L/C* images. Hence, both high relief and uniformly flat areas appear dark in *L/C* images. In contrast, areas where cover is too thick to be penetrated by *C* band but not too thick for *L* band penetration have high *L/C* and appear as whitish areas.

L and *C* bands with different polarizations, *X* band, and *L/C* ratio of bands with different polarizations were used to generate color-composite, multiband SIR C/X SAR images, and two of the better resolved of these combinations are shown in plate 1. These images allow different wavelengths and polarizations to be displayed in a single image. Plate 1a shows the excellent definition that results from co-registration of *L*, *C*, and *X* bands. Note that *L* images are the best for outlining structural details in the Keraf Suture, and that cross-polarization enhances the penetration capability of *C* band. Hence a false-color image produced from L_{hh}, L_{hv}, and C_{hv} also results in excellent structural definition (Plate 1b). These images are not superior to the black and white, single-band *L* images in revealing basement structures. They do, however, have the advantage of displaying both basement structures and morphology, as they include the shorter wavelength *C* and *X* bands where backscattering from rough surfaces dominates over penetration and volume scattering.

Interpretation of SIR-C/X-SAR Imagery of the Southern Keraf Suture

The tone and texture of the SIR C/X SAR images are due to differences in backscattering of radar waves due to varying surface and subsurface roughness and relief, which in turn,

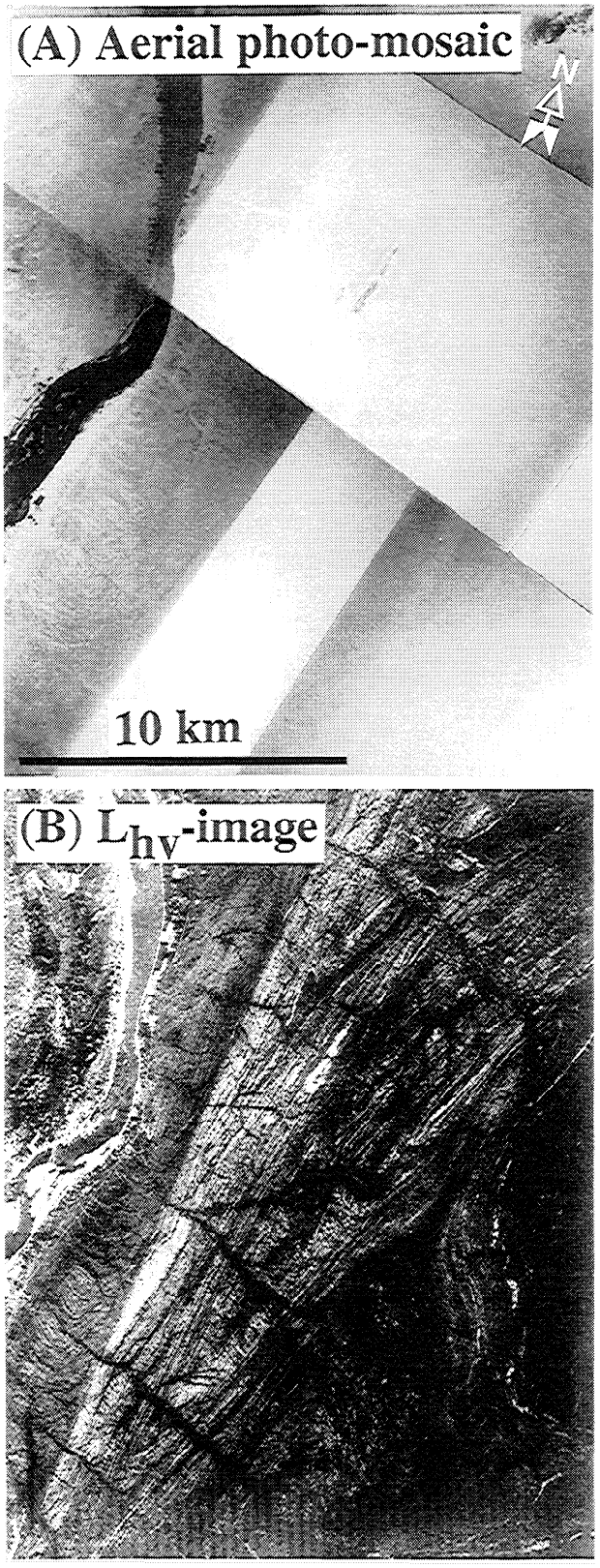

Figure 6. (a) The 1:70 000 scale aerial photograph mosaic, and (b) black and white, single-band (L_{hv}) SIR-C/X-SAR image over the 18 x 23 km test area in the Keraf Suture. Location of the test area is shown in Figure 3. Note the remarkable difference in basement structures illuminated in the *SIR C/X SAR* image, which are not apparent in the aerial photograph mosaic. The dark spot in the upper right corner is a printing artifact. The only outcrop visible in the aerial photograph mosaic is the narrow, N-trending ridge in the upper center of the mosaic.

reflect differences in susceptibility of different lithologies to weathering and erosion. Hence tonal and textural variation in the SIR C/X SAR images can be used to map lithologic units. Granitic bodies in the Keraf Suture form isolated peaks (Figure 5a) with sharp relief compared to the surrounding plain. These plutonic bodies appear as bright patches in the SIR C/X SAR images (labeled A in Figure 9b). Orthogneiss in the Bayuda Desert, west of the Keraf Suture form low-lying, rough, and hilly terrain. These rocks appear in the SIR C/X SAR images as areas with diffused dark and bright tones with no discernible pattern (labeled B in Figure 9b). Alternatively, paragneiss intercalated with carbonates and amphibolites lying east of the Keraf Suture form areas of subdued relief defined by differentially eroded layers with sharp local relief (Figure 5c). These appear as successions of dark and bright bands on the SIR C/X SAR images (labeled c in Figure 9b). Unmetamorphosed, but deformed syntectonic sediments also exhibit this pattern in the SIR C/X SAR images (labeled D in Figure 9b). However, fold geometry, and the spacing, continuity, and thickness of dark and bright bands in the SIR C/X SAR images (labeled E in Figure 9b) enable differentiation between layered metamorphic assemblages and bedded unmetamorphosed, but deformed sediments. Ultramafic rocks in the Keraf Suture (outside the area covered by Figure 9) form curvilinear ridges. These appear as bright linear bands in the SIR C/X SAR images.

Structural features in the SIR C/X SAR images are defined by trends of alternating dark and bright bands which correspond to bedding. Closure of major folds are defined by curvatures in these bands (labeled E in Figure 9b). Axial traces of folds are constructed by connecting points of maximum curvature in adjacent beds. The geometry of fold hinge zones (angular, rounded, box) is well-defined on the SIR C/X SAR images. However, determining the three-dimensional geometry of the folds (plunge of hinge line, attitude of the axial surface, and attitude of the limbs) is not possible based on imagery alone. The structures of the Keraf Suture are too low-lying for dip direction to be obtained from radar "shadow". The geometry of folds can be deduced in some cases where folds deform thrusts planes (labeled F in Figure 9b) and unconformities (labeled G in Figure 9b). Since vergence and geometry of folds in the case are known, the asymmetry of these folds can be used to define the sense of shear across major strike-slip faults.

Near-vertical faults appear as sharp, linear feaures in the SIR C/X SAR images. This is because faults in the Keraf area are defined by narrow (~50 m wide) ridges of mylonitized granite. Strike-slip faults mark sharp boundaries (labeled H in Figure 9b), the planar fabric on either sides of them are either sharply truncated or sheared off (labeled I and J in Figure 9b). Shear sense is deduced from the asymmetry of folded fault surfaces and other folded planar features. The major strike-slip fault in the center of Figure 9 has a left-lateral sense of shearing as deduced from the geometry of the folded thrust fault exposed to the west at the base of the Amaki Series (labeled F in Figure 9b).

Structural Features of the Southern Keraf Suture

Interpretation of the SIR C/X SAR images and field data enable structures in the southern Keraf Suture to be mapped for the first time. Figure 10 outlines the major structural features in the southern Keraf Suture, along with the previously mapped Abu Hamed Interference Fold and the Dam et Tor Fold/Thrust

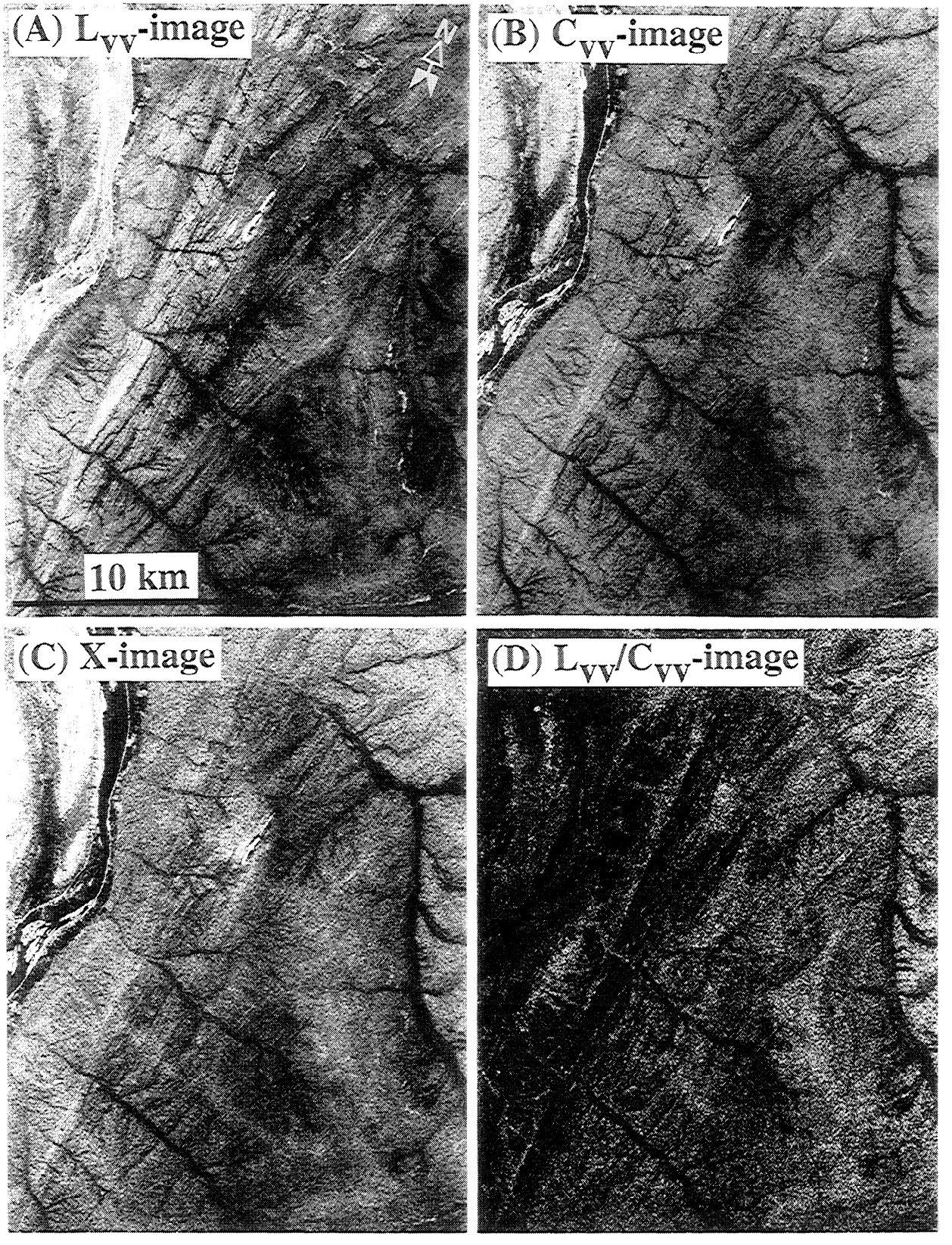

Figure 7. Comparison between black and white, single-band and ratio-band SIR C/X SAR images covering the same area in the Keraf Suture: (a) L_{VV} image, (b) C_{VV} image, (c) X image, and (d) L_{VV}/C_{VV} image. Structures are best revealed by longer wavelengths in the relative order (best to worst) L_{VV}, C_{VV}, and X image. This is attributed to the greater penetration of longer wavelengths in dry sand. Comparing the L_{VV}/C_{VV} image with the L_{VV}, C_{VV}, and X image allows qualitative mapping of relative penetration by L_{VV} band. For example, areas where sand cover is too thick to be penetrated by C_{VV} band but not too thick for L_{VV} band penetration, have high L_{VV}/C_{VV} ratio, and appear as whitish areas.

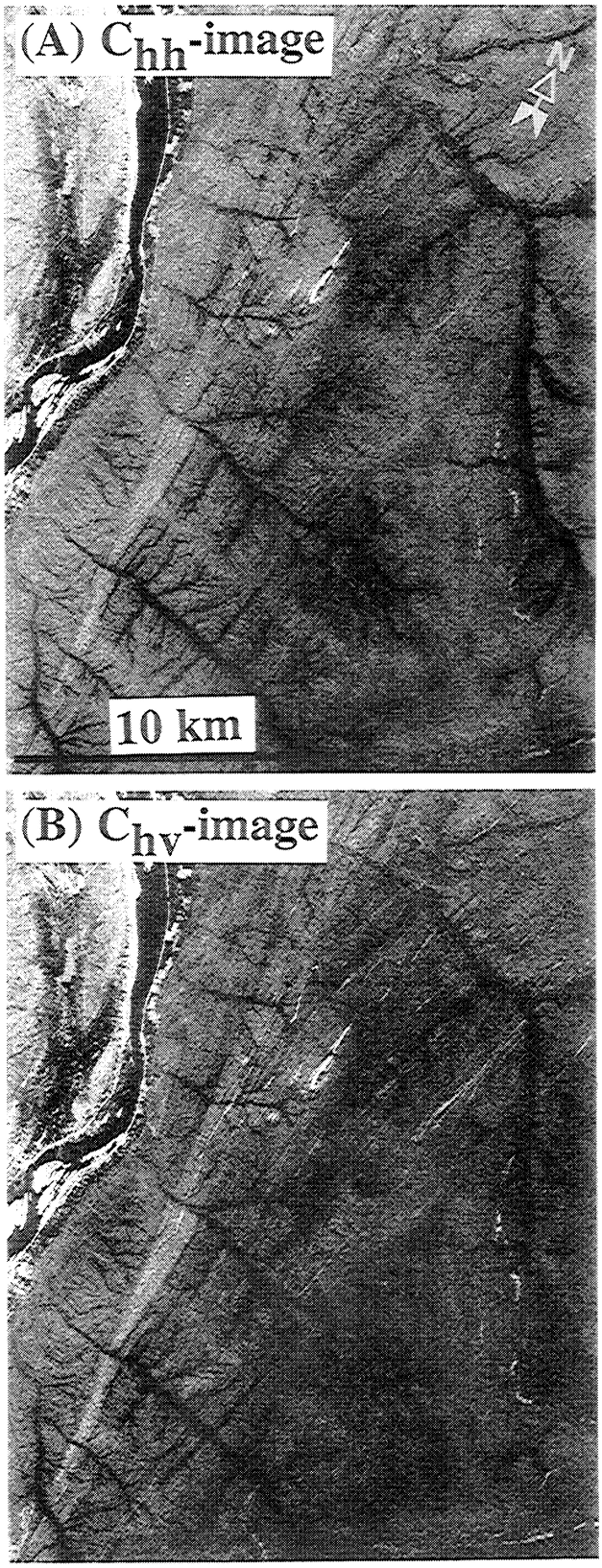

Figure 8. A comparison between C images of different polarizations covering the same area in the Keraf Suture: (a) C_{hh} image, and (b) C_{hv} image. Cross polarization (hv) enhances penetration of the C band. This is evident by the better illumination of structural details in the C_{hv} image compared to absence of such details in the C_{hh} image.

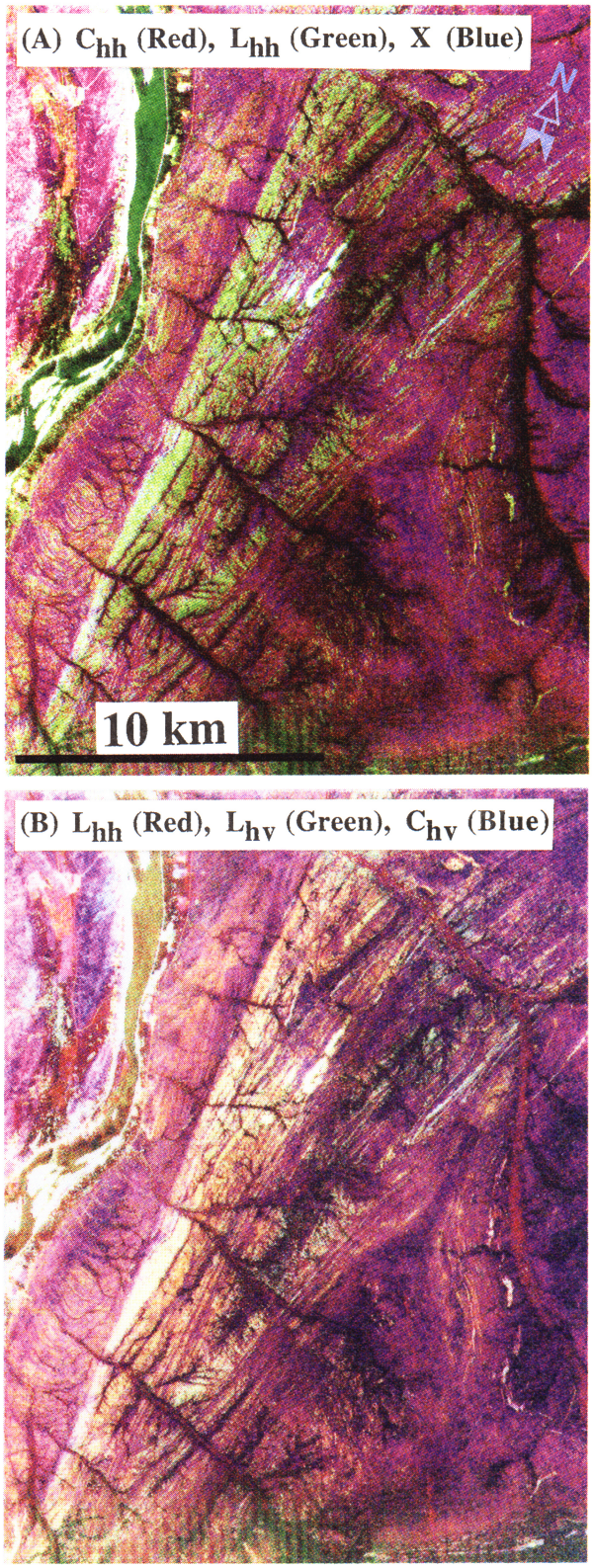

Plate 1. A comparison between color-composite, multiband SIR C/X SAR images covering the same area in the Keraf Suture: (a) C_{hh} (red), L_{hh} (green), and X (blue), and (b) L_{hh} (red), L_{hv} (green), and C_{hv} (blue). The color-composite, multiband SIR C/X SAR images resolves structural details as well as drainage. This is due to the usage of bands with different wavelengths and polarizations.

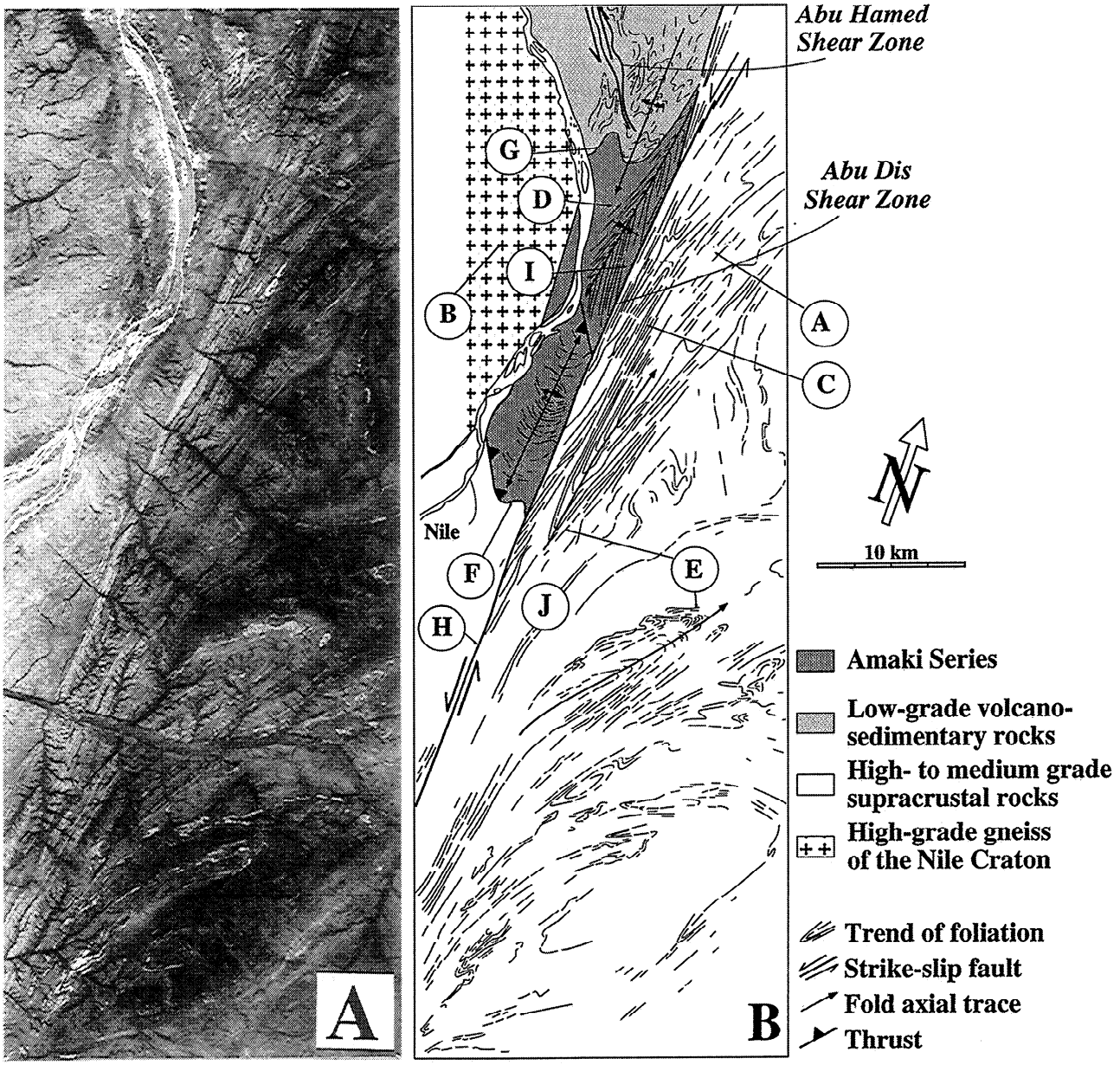

Figure 9. (a) A L_{tp} image showing recognizable lithological and structural features in part of the Keraf Suture, and (b) Interpretation of the image. Labels in the map are explained in the text.

Belt in the Bayuda Desert. This map is based on interpretation of a mosaic of L_{tp}-images (tp being total power) generated from three SIR C/X SAR data takes (SRL-1 50.4 and 82.42, SRL-2 82.42), supplemented by 3 weeks of field studies. The following interpretation builds on the analysis of *Abdelsalam et al.* [1995], who identified two phases of pre-Keraf-age deformation related to N-S shortening reflecting closure of the NE-SW trending Atmur-Delgo suture followed by three phases of Keraf-age deformation that resulted in the formation of N-S structures. The tectonic history of the southern Keraf Suture is different in many details from that of the northern Keraf Suture, but both the north and south Keraf Suture are similar, in that older E-W "pre-Keraf-age" structures are overprinted by younger N-S Keraf-age structures.

Pre-Keraf-Age Structures

Pre-Keraf-age structures are best preserved immediately west of the Keraf Suture, in the Bayuda Desert. This region is dominated by medium- to high-grade gneiss and deformed, metamorphosed supracrustal rocks. The E- to NE-trending structures in the Bayuda Desert include the Abu Hamed Interference Fold in the north and the Dam et Tor Fold/Thrust Belt in the south (Figure 10). These become increasingly deformed by Keraf-age structures near the Keraf Suture where they are refolded and then truncated. These relations indicate that the E- and NE-trending structures in the Bayuda Desert are older than the N-S structures of the Keraf Suture.

The Abu Hamed Interference Fold lies in the northeasternmost part of the Bayuda Desert, where the Nile

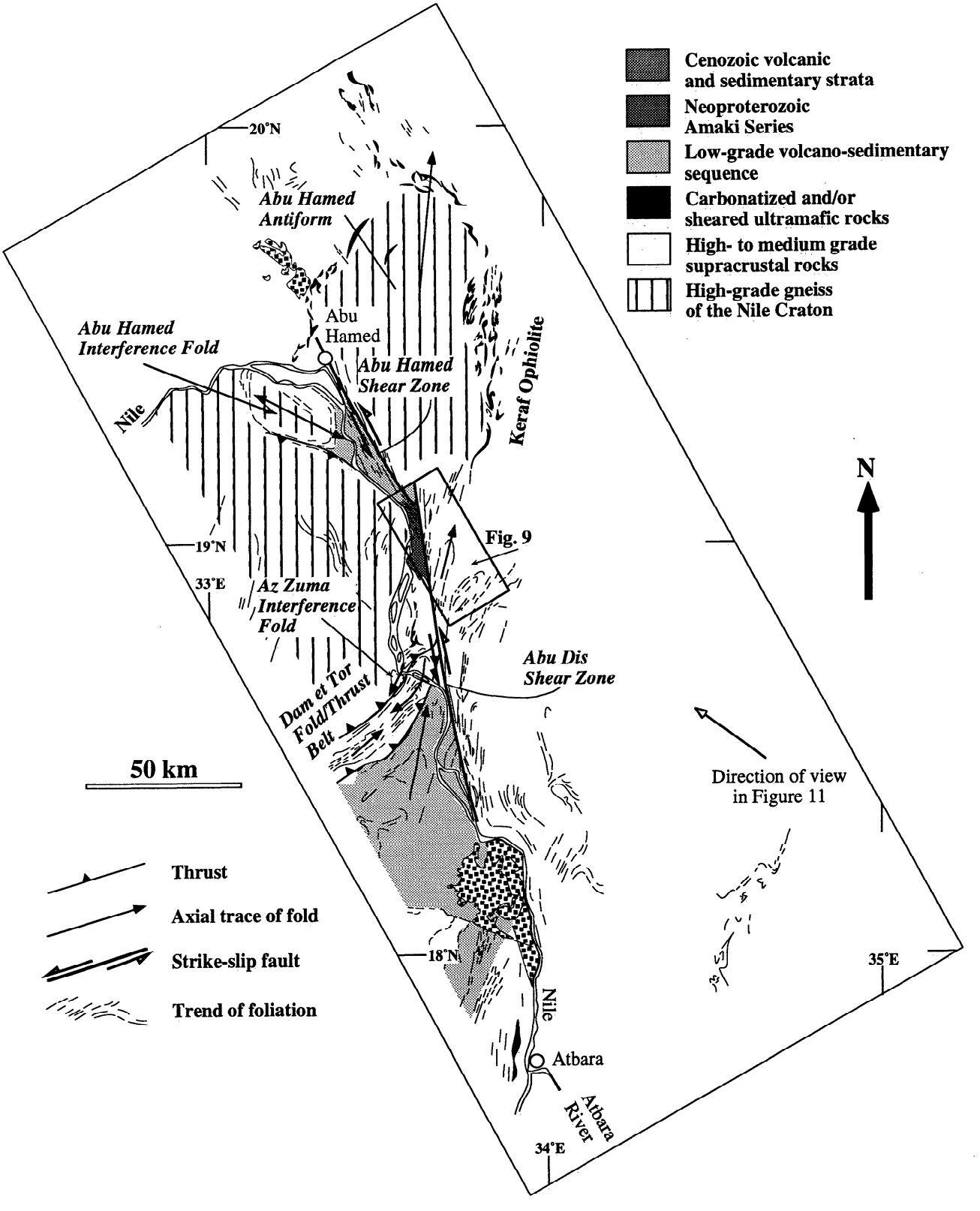

Figure 10. A map showing the main structural features in the southern Keraf Suture. The map is based on the interpretation of a L_{tp} image mosaic from three SIR C/X SAR data takes. See text for discussion.

River begins its great bend to the southwest (Figure 10). This structure occupies an area of about 200 km^2 and is defined by a core of biotite-hornblende gneiss surrounded by layered supracrustal rocks including pelitic and graphitic schists, marble and quartzite [*Ries et al.*, 1985]. This structure is a dome developed as an E-trending pre-Keraf-age antiform was refolded by a N-trending Keraf-age antiform (Figure 10). This dome is bounded to the south by a N-verging thrust (Figure 10)

which deforms talc-carbonate schist. Shortening across the thrust resulted in emplacement of quartzofeldspathic gneiss of the Bayuda Desert over the supracrustal rocks of the Abu Hamed Interference Fold. To the east, rocks of the Abu Hamed Interference Fold are overlain by a triangular body of low-grade, greenschist facies volcano-sedimentary rocks (Figure 10). The contact between the rocks of the Abu Hamed Interference Fold and the low-grade volcano-sedimentary rocks is not certain, but *Vail* [1988] suggested that this contact was defined by a W-verging thrust. If this interpretation is correct, the low-grade rocks are a thrust nappe, perhaps a tectonic outlier derived from the ANS.

The Abu Hamed Interference Fold is an E-trending antiform. The eastern end of the antiform plunges shallowly (~5°) to the east. Mapping by *Meinhold* [1979] and *Ries et al.* [1985] suggest that the western part of the fold plunges to the west. The E-trending antiform deforms foliations and intrafolial folds. These have various orientations depending on their position with respect to the antiform. Complex interference folds developed when older intrafolial folds were refolded by parasitic second- and third- order folds associated with the E-trending antiform. A set of younger N- and S-plunging cross-folds deform foliations folded by the E-trending antiform and axial planar cleavage associated with its development. These cross-folds are apparent on the southern limb of the E-trending antiform and the N-verging thrust further south. We interpret the N- and S-plunging fold to be related to an open N-trending antiform which was superimposed on the older E-trending antiform, producing the dome cored by the biotite-hornblende gneisses and rimmed by supracrustal rocks.

The Dam et Tor Fold/Thrust Belt occupies the east-central part of the Bayuda Desert where it extends in a NE-SW-direction for over 40 km (Figure 10). Rocks in the Fold/Thrust belt consist of high-grade supracrustal rocks dominated by garnet and kyanite schists. They are separated from greenschist facies volcaniclastic rocks by a SE-verging thrust (Figure 10). *Meinhold* [1979] interpreted these low-grade rocks of the Bayuda Desert as being retrograde equivalents of the surrounding high-grade rocks. Alternatively, *Vail* [1988] interpreted the low-grade rocks as allochthonous and derived from the east. The northern boundary of the Dam et Tor Fold/Thrust Belt is defined by another SE-verging thrust which juxtaposes the Dam et Tor structures against the Az Zuma Interference Fold (Figure 10).

The central part of the Dam et Tor Fold/Thrust Belt contains a NE-trending, doubly plunging basin (Figure 10). The basin is bounded by the thrusts in the Dam et Tor Belt (Figure 10). To the north of the basin structure, the Az Zuma Interference Fold (Figure 10) crops out as a mushroom-shaped structure which plunges to the SW. The Dam et Tor basin structure may have resulted from superimposition of a N-trending synform on an older NE-trending synform, whereas the Az Zuma structure resulted from the superimposition of a N-trending Keraf-age antiform on an older NE-trending pre-Keraf-age synform.

The Dam et Tor Fold/Thrust Belt continues NE for ~5 km east of the Nile Nile before it is truncated by the Abu Dis Shear Zone (Figure 10). The Abu Dis Shear Zone is the most prominent structure in the southern Keraf Suture. The southern part of the Abu Dis Shear Zone defines the eastern boundary of the volcano-sedimentary domain to the south of the Dam et Tor Fold/Thrust Belt (Figure 10). N-plunging, tight folds, possibly developed during left-lateral strike-slip movement along the Keraf Suture (discussed below) deform the low-grade volcano-sedimentary domain, and further indicate that the emplacement of the volcano-sedimentary rocks predates Keraf-age deformation.

Keraf-Age Structures

The structural style of the Keraf Suture varies significantly along its strike. Structures in north of Abu Hamed are dominated by upright folds manifesting E-W-shortening [*Abdelsalam et al.*, 1995]. In contrast, deformation in the southern Keraf Suture is dominated by N- and NNW-trending left-lateral strike-slip faults and shear zones. A major antiform, the Abu Hamed Antiform (Figure 10), occupies the transition between the northern and southern Keraf Suture.

Although the eastern and western limits of the northern Keraf Suture are well defined, the location and nature of the eastern boundary of the southern Keraf Suture are not nearly as apparent. In the north, Keraf-age deformation is confined to a ~50 km wide belt of carbonate-rich turbidites [*Abdelsalam et al.*, 1995]. These are bounded to the east by arc-derived volcanic rocks of the Gabgaba terrane (Figure 2). The medium- to high-grade gneiss terrane of the Nile Craton defines the western boundary of the north and south Keraf Suture (Figure 2). The western boundary of the southern Keraf Suture is well-marked by the previously mentioned left-lateral strike-slip faults (Figure 10).

Supracrustal rocks in the Keraf Suture give way to the arc volcanics of the Gebeit terrane to the east, and appears to be ~50 km wide. However, the exact location and nature of the contact between the Keraf Suture and the ANS cannot be resolved in the radar images we studied. In the following, we outline the structural features in the southern Keraf Zone. The major structural features of the southern Keraf Suture are presented and interpreted in light of our understanding of the northern Keraf Suture.

The Abu Hamed Antiform lies NNE of the town of Abu Hamed (Figure 10) and occupies an area of about 3500 km^2. The antiform is bounded in the south by amphibolite facies metasediments and paragneiss. Predominantly low-grade carbonate-rich turbidites lie to the north. The Abu Hamed Antiform plunges ~40° to the north and verges to the W. The core of the Antiform is dominated by quartzofeldspathic gneiss and foliated granite. These are surrounded by low-grade greenschist facies metamorphic rocks including immature volcanogenic sediments such as polymict conglomerates and highly sheared ultramafic rocks (Figure 10). The ultramafic rocks are interpreted as dismembered ophiolites [*Abdel-Rahman et al.*, 1993]. The ultramafic rocks and the volcanogenic sediments are separated from the quartzofeldspathic gneiss by a deformed thrust. We interpret these relationships to indicate that the low-grade assemblages were thrust from the east over the quartzofeldspathic gneiss before being deformed together about the N-plunging antiform.

The Abu Hamed Shear Zone is a ~70 km long, NNW-trending system of left-lateral strike-slip faults and shear zones which lies just east of the Nile River on the western margin of the Abu Hamed Antiform (Figure 10). The central part of the shear zone is dominated by brittle deformation. However, the northern end of the shear zone has ductiley transposed the western limb of the Abu Hamed Antiform before dying out to the north (Figure 10). The northern Abu Hamed Shear Zone is defined by a ~50 m wide zone of well-developed

mylonitic rocks which dip steeply to the west. A sub-horizontal, N-plunging stretching lineation defined by elongated mineral grains is contained in the sub-vertical foliation. The eastern edge of the shear zone is defined by planar fabric folded about N-trending axes. The Abu Hamed Shear Zone widens to the south and is defined by a ~500-m-wide zone of mylonitic rocks which is deflected to the east before being truncated against the Abu Dis Shear Zone (Figure 10).

The Abu Dis Shear Zone is a N-trending system of faults and shear zones which extends south of the Abu Hamed Shear Zone for more than 150 km along the eastern bank of the Nile River (Figure 10). The northern part of the shear zone truncates the western limb of the Abu Hamed Antiform and dies out further north in the rocks of its gneissic core. The southern end of the shear zone bends west where it crosses the Nile and disappears under the Umm Arafibia volcanic field (Figure 3). NNE-trending structures continue south of the volcanic field and may represent the continuation of the Abu Dis Shear Zone; alternatively, these structures may represent another structural manifestation of the Keraf Suture. The Abu Dis Shear Zone is defined by a narrow (~50 m) band of mylonitic granite. The mylonite fabric dips west and contains a stretching lineation that plunges gently to the south. The region to the east of the Abu Dis Shear Zone is dominated by NNE-trending, tight folds which verge to the west (Figure 9). These folds are interpreted as indicating NW-SE shortening, possibly associated with the major left-lateral strike-slip movement along the Abu Dis Shear Zone.

Folded but unmetamorphosed sandstone and conglomerate are exposed west of the Abu Dis Shear Zone (Figure 9) and were named the "Amaki Series" by *Dawoud* [1980] from exposures west of the Nile River. SIR C/X SAR imagery has revealed that the Amaki series is also extensively exposed east of the Nile River. The Amaki Series is made up of immature, poorly sorted pebbly sandstone and conglomerate. Clasts in the conglomerate are predominantly (~90%) composed of pink granite. These sediments form a ~30 km long and ~5-km-wide, elongated N-trending wedge which occupies a synformal basin that abuts the Abu Dis Shear Zone. The southern boundary of the wedge is a S-verging thrust which emplaced Amaki Series over high-grade paragneiss as evident by kinematic indicators from along the fault contact. The northern boundary of the basin is a folded depositional contact which overlies low-grade volcano-sedimentary rocks. The western boundary of the wedge lies along the course of the Nile River and is not well exposed. The northern part of the Amaki Series is deformed into a S-plunging chevron-type synform whereas the southern part is deformed into open basin-dome interference folds (Figure 9).

Tectonic Evolution of the Southern Keraf Suture

The northern Keraf Suture has been traced for over 250 km, from near the Sudanese-Egyptian border south to the vicinity of Abu Hamed (Figure 2) [*Almond and Ahmed*, 1987; *Abdel-Rahman et al.*, 1993; *Abdelsalam et al.*, 1995]. SIR C/X SAR images permit us to extend the southern Keraf Suture for another 300 km from Abu Hamed south along the Nile River to Atbara (Figure 2), making it the longest continuous basement structure in NE Africa. The Keraf Suture maintains a uniform width of ~50 km throughout this length and is interpreted as a major suture between the ANS in the east and the Nile Craton to the west for the following reasons; (1) The Keraf Suture is a major lithospheric feature which separates crustal blocks with distinct geochronological and isotopic characteristics, continental to the west and oceanic to the east [*Almond and Ahmed*, 1987; *Stern and Kröner*, 1993; *Stern et al.*, 1994]. (2) Presence of ultramafic fragments along the Keraf Suture indicates closure of oceanic crust [*Abdel-Rahman et al.*, 1993]. (3) Subsequent Keraf-age deformation involved a collapsed, ancient continental margin. These three observations are consistent with a suture between a continent and a composite arc terrane [*Vail*, 1983]. However, the structural style in the Keraf Suture is different from arc-continental sutures exposed elsewhere between the ANS and the Nile Craton such as the Kabus Suture in central Sudan [*Abdelsalam and Dawoud*, 1991] and the Sekerr suture in northern Kenya [*Shackleton*, 1986]. Moreover, structural styles differ between the northern and southern Keraf Suture. The evolution of the northern Keraf Zone is outlined by *Abdelsalam et al.* [1995]. The evolution of the southern Keraf Zone can be broadly summarized into three deformational phases:

1. Continental crust of the Nile Craton was deformed prior to collision along the Keraf Suture. Early deformation is associated with development of the E-trending Abu Hamed Interference Fold and the NE-trending Dam et Tor Fold/Thrust Belt. These and other E- and NE- trending structures west of the Keraf Suture were developed in response to a N-S shortening, perhaps related to closure of the Atmur-Delgo oceanic re-entrant (Figure 11a) [*Schandelmeier et al.*, 1994].

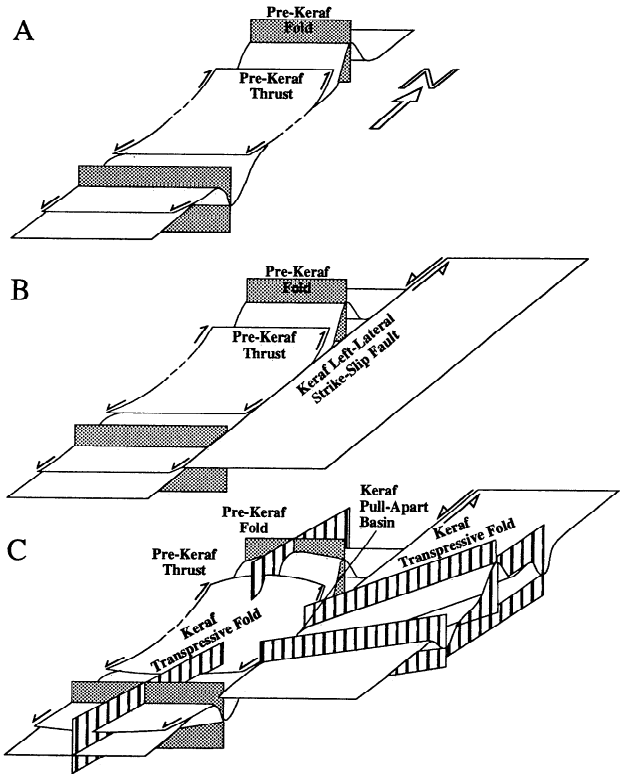

Figure 11. A three-dimensional cartoon summarizing the structural evolution of southern Keraf Suture: (a) Development of E- to NE-trending structures as a result of N-S shortening, (b) Development of the N- to NNW-trending left-lateral strike-slip faults in the Keraf Suture, and (c) Development of N- to NE-trending transpressional folds and the Amaki transtensional basin.

2. The continental slope and basin between the Nile Craton and the ANS was the site of both clastic and carbonate sedimentation. The subsequent collision was associated with metamorphism that formed a belt of paragneiss and marble along the Keraf Suture. Early stages of collision may have resulted in emplacement of thrust sheets of volcanogenic sediments and ophiolites westward over the easternmost Nile Craton, where they are now well-exposed around the Abu Hamed Antiform.

3. Continued oblique convergence resulted in a system of left-lateral shear zones. The presence of N- to NNW-trending left-lateral strike-slip faults in the southern Keraf Suture suggests that shortening associated with the collision between the ANS and the Nile Craton may have been accompanied by a significant strike-slip component (Figure 11b). Similar conclusions have been reached by workers in other parts of the East African Orogen [*Shackleton*, 1986; *Drury and Berhe*, 1993; *Wallbrecher et al.*, 1993]. The Amaki basin may reflect a local transtensional environment accompanying oblique convergence (Figure 11c). Syntectonic sediments were derived mainly from granites exposed near or along the faults and were deformed by continued left-lateral strike-slip faulting. E-W to NW-SE-directed shortening is also associated with the Keraf Suture where it is expressed as N- to NE-trending folds. These were superimposed on the earlier E- to NE-trending folds to the west of the Keraf Zone and produced the Abu Hamed Interference Fold and structures in the central part of the Dam et Tor Fold/Thrust Belt.

The structural style apparent along the Keraf Suture is consistent with oblique collision or convegence. In the northern Keraf Suture, collision was accommodated by N-trending folds and lesser NW-trending, left-lateral and NE-trending, right-lateral strike-slip faults [*Abdelsalam et al.*, 1995]. However, in the southern Keraf Suture, deformation is dominated by left-lateral strike-slip faults as exemplified by the Abu Hamed and the Abu Dis Shear Zones. This style of strain dies out to the north where N- to NNW-trending left-lateral strike-slip movement translated into dominantly E-W shortening, as exemplified by the Abu Hamed Antiform.

Conclusions

1. SIR C/X SAR images spectacularly reveal basement structures obscured by extensive aeolian cover in the Sahara Desert. Structures are best revealed by longer wavelengths, in relative order (best to worst) of *L* band, *C* band, and *X* band. This is attributed to the greater penetration of longer wavelengths in dry sand. In addition, cross-polarization enhances penetration of *C* band radar.

2. Studies based on combined SIRA and SIR C/X SAR imagery have extended the known length of the Keraf Suture by more than 300 km, making it the longest basement structure in NE Africa.

3. Deformation in the southern Keraf Suture is dominated by N- to NNW-trending left-lateral strike-slip faults developed in response to a NW-SE compression. These faults truncate the older E- to NE-trending structures in the Nile Craton to the west. Both N- to NE-trending folds and possibily a transtensional basin are associated with the left-lateral strike-slip faults. Structural styles in the Keraf Suture differ in that the northern part is dominated by N-trending upright folds which imply E-W shortening. However, structures in the northern and southern Keraf Suture are associated with both left-lateral strike-slip and thrust faulting. This suggests oblique convergence when the ANS was sandwiched between colliding continental fragments of East and West Gondwana.

Acknowledgments. This work was supported by NASA through the Jet Propulsion Laboratory. The authors would like to thank the Geological Research Authority of the Sudan for their co-operation and help during the field phase of this work. Thanks are also due to E. Elfaki, B. Elhur, and F. Ibrahim for their assistance in the field. We also gratefully acknowledge the assistance of A. Daniels and S. Okonek in processing the images. We would also like to thank K. Mueller and M. Sultan for reviewing the manuscript. Programs in Geosciences contribution 828.

References

Abdel-Rahman, E.S.M., Geochemical and Geotectonic Controls of the Metallogenic Evolution of Selected Ophiolite Complexes from the Sudan. *Berlin. Geowiss. Abh.,145*, 175#pp., 1993.

Abdel-Rahman, E.M., U. Harms, H. Schandelmeier, G. Franz, D.P.F. Darbyshire, P. Horn, and D.A. Muller-Sohnius, A new ophiolite occurrence in NW Sudan - Constraints on late Proterozoic tectonism, *Terra Nova, 2*, 363-376, 1990.

Abdel-Rahman, E.M., G. Matheis, H. Schandelmeier, M.A. Karfis, I. Abdel-Gadir, and M. El-Khedir, Evolution of the Keraf back-arc basin: Constraints on the Nubian Shield margin. in *Geoscientific Research in NE Africa*, edited by U. Thorweihe, and H. Schandelmeier, pp. 93-98, A.A. Balkema, Brookfield, Vt., 1993.

Abdelsalam, M.G., and A.S. Dawoud, The Kabus ophiolitic melange, Sudan, and its bearing on the W boundary of the Nubian Shield, *J. Geol. Soc. London, 148*, 83-92, 1991.

Abdelsalam, M.G., R.J. Stern, H. Schandelmeier, and M. Sultan, Deformational history of the Keraf Zone in NE Sudan, revealed by Shuttle Imaging Radar, *J. Geol., 103*, 475-491, 1995.

Almond, D.C., and F. Ahmed, Ductile shear zones on N Red Sea Hills, Sudan and their implication for crustal collision, *Geol. J., 22*, 175-184, 1987.

Barth, H., C. Besang, H. Lenz, and K-D. Meinhod, Results of petrological investigations and Rb/Sr age determinations on the non-orogenic igneous ring complexes in the Bayuda Desert, Sudan, *Geol. Jahrb., B51*, 3-34, 1983.

Burke, H., and C. Sengor, Tectonic escape in the evolution of the continental crust, in *Reflection Seismology: The Continental Crust*, edited by M. Barazangi, and L. Brown, pp. 41-53, Am. Geophys. Union, Geodyn. Ser. , 14, Washington, D.C., 1986.

Dawoud, A.S., Structural and metamorphic evolution of the area southwest of Abu Hamed, Nile Province, Sudan, Ph.D. thesis, 175#pp., Univ. of Khartoum, 1980.

Denkler, T., G. Franz, and H. Schandelmeier, Tectono-metamorphic evolution of the Neoproterozoic Delgo suture zone, Northern Sudan, *Geol. Rundsch., 83*, 578-590, 1994.

Dixon, T.H., and M.P. Golombek, Late Precambrian crustal accretion rates in NE Africa and Arabia, *Geology, 16*, 991-994, 1988.

Drury, S.A., and S.M. Berhe, Accretion tectonics in northern Eritrea revealed by remotely sensed imagery, *Geol. Mag., 130*, 177-190, 1993.

Harms, U., H. Schandelmeier, and D.P.F. Darbyshire, Pan-African reworked early/middle Proterozoic crust in NE Africa W of the Nile: Sr and Nd isotope evidence, *J. Geol. Soc. London, 147*, 859-872, 1990.

Harms, U., D.P.F. Darbyshire, T. Denkler, M. Hengst, and H. Schandelmeier, Evolution of the Neoproterozoic Delgo suture zone and crustal growth in Northern Sudan geochemical and radiogenic isotope constraints, *Geol. Rundsch., 83*, 591-603, 1994.

Harris, N.B.W., C.J. Hawkesworth, and A.C. Ries, Crustal evolution in NE and E Africa from model Nd ages, *Nature, 309*, 773-776, 1984.

Key, R.M., T.J. Charsley, B.D. Hackman, A.F. Wilkinson, and C.C. Rundle, Superimposed Upper Proterozoic collision-controlled orogenies in the Mozambique Orogenic Belt of Kenya, *Precambrian Res., 44*, 197-225, 1989.

McCauley, J.F., G.G. Schaber, C.S. Breed, M.J. Grolier, C.V. Haynes, B. Issawi, C. Elachi, and R. Blom, Subsurface valleys and geoarcheology of the Eastern Sahara revealed by Shuttle Radar, *Science, 218*, 1004-1020, 1982.

Meinhold, K-D., The Precambrian basement complex of the Bayuda Desert, Northern Sudan. *Rev. Geol. Geogr.Phys., 21,* 395-401, 1979.

Muhongo, S., and J-L. Lenoir, Pan-African granulite-facies metamorphism in the Mozambique Belt of Tanzania: U-Pb zircon geochronology, *J. Geol. Soc. London, 151,* 343-347, 1994.

Raisz, E., *Landform Map of North Africa,* scale 1:5,000,000., Environ. Prot. Branch, Quartermaster General, U.S. Army, Washington, D.C., 1952.

Ries, A. C., R.M. Shackleton, and A.S. Dawoud, Geochronology, geochemistry and tectonics of the NE Bayuda Desert, northern Sudan: Implication for the western margin of the late Proterozoic Fold Belt of NE Africa, *Precambrian Res., 30,* 43-62, 1985.

Sandford, K.S., Notes on the Nile Valley in Berber and Dongola, *Geol. Mag., 86,* 97-109, 1949.

Schandelmeier, H., D.P.F. Darbyshire, U. Harms, and A. Richter, The E Saharan craton: Evidence for pre-Pan-African crust in NE Africa W of the Nile, in *The Pan-African Belts of NE Africa and Adjacent Areas,* edited by S. El Gaby, and R.O. Greiling, pp. 69-94, Friedr Vieweg and Sohn, Braunschweig, Ger., 1988.

Schandelmeier, H., E. Eipfler, D. Küster, M. Sultan, R. Becker, R.J. Stern, and M.G. Abdelsalam, Atmur-Delgo suture: A Neoproterozoic oceanic basin extending into the interior of northeast Africa. *Geology, 22,* 563-566, 1994.

Shackleton, R.M., Precambrian collision tectonics in Africa, in Collision Tectonics, edited by M.P. Coward, and A.C. Ries, A.C, *Geol. Soc London Spec. Publ., 19,* 329-349, 1986.

Stern, R.J., Arc assembly and continental collision in the Neoproterozoic E African Orogen: Implication for the consolidation of Gondwanaland, *Ann. Rev. Earth Planet. Sci., 22,* 319-351, 1994.

Stern, R.J., and A. Kröner, Geochronologic and isotopic constraints on the late Precambrian crustal evolution in NE Sudan, *J. Geol., 101,* 555-574.1993.

Stern, R.J., M.G. Abdelsalam, H. Schandelmeier, and M. Sultan, Carbonates of the Bailateb group, NE Sudan: a Neoproterozoic (ca. 750 Ma) passive margin on the eastern flank of west Gondwanaland?, *Geol. Soc. Am. Abstr. Programs, 27,* 49, 1993.

Stern, R.J., A. Kröner, T. Reischmann, R. Bender, and A.S. Dawoud, Precambrian basement around Wadi Halfa: A new perspective on the evolution of the East Saharan Craton, *Geol. Rundsch., 83,* 564-577, 1994.

Stoeser, D.B., and J.S. Stacey, Evolution, U-Pb geochronology, and isotope geology of the Pan-African Nabitah orogenic belt of the Saudi Arabian Shield, in *The Pan-African Belts of NE Africa and Adjacent Areas,* edited by S. El Gaby, and R.O. Greiling, pp. 227-288, Friedr Vieweg and Sohn, Braunschweig, Ger., 1988.

Sultan, M., K.R. Chamberlin, S.A. Bowring, R.E. Arvidson, H. Abuzied, and B. EL-Kaliouby, Geochronologic and isotopic evidence for involvement of pre-Pan-African crust in the Nubian Shield, Egypt, *Geology, 18,* 761-764, 1990.

Sultan, M., M.E. Bickford, B. El-Kaliouby, and R.E. Arvidson, Common Pb systematics of Precambrian granitic rocks of the Nubian Shield (Egypt) and tectonic implications, *Geol. Soc. Am. Bull., 104,* 456-470, 1992.

Sultan, M., R. Becker, R.E. Arvidson, P. Shore, R.J. Stern, Z. El-Alfy, and R.I. Attia, New constraints on Red Sea Rifting from correlations of Arabian and Nubian Neoproterozoic outcrops, *Tectonics, 12,* 1303-1319, 1993.

Sultan, M., R.D. Tuckler, Z. El-Alfy, R.I. Attia, and A.I. Ragab, U-Pb (zircon) ages for the gneissic terrane west of the Nile, southern Egypt, *Geol. Rundsch., 83,* 514-522, 1994.

Vail, J.R., Pan-African crustal accretion in NE Africa, *J. Afr. Earth Sci.,1,* 285-294, 1983.

Vail, J.R., Pan-African (late Precambrian) tectonic terranes and reconstruction of the Arabian-Nubian Shield, *Geology, 13,* 839-842, 1985.

Vail, J.R, Tectonics and evolution of the Proterozoic basement of NE Africa, in *The Pan-African Belts of NE Africa and Adjacent Areas,* edited by S. El Gaby, and R.G. Greiling, pp. 185-226, Friedr. Vieweg and Sohn, Braunschweig, Ger., 1988.

Wallbrecher, E., H. Fritz, A.A. Khudeir, and F. Farahad, Kinematics of Pan-African thrusting and extension in Egypt, in *Geoscientific Research in NE Africa* edited by U. Thorweihe, and H. Schandelmeier, pp. 27-30, A.A. Balkema, Brookfield, Vt., 1993.

M.G. Abdelsalam and R.J. Stern, Center for Lithospheric Studies, University of Texas at Dallas, Box 830688, MS FA 31, Richardson, TX 75083-0688.

(Received October 16, 1995; revised February 25, 1996; accepted April 29, 1996.)